The Astronomical Journal, 153:196 (15pp), 2017 April https://doi.org/10.3847/1538-3881/aa6624

A 2MASS/AllWISE Search for Extremely Red L Dwarfs: The Discovery of Several Likely L Type Members of β Pic, AB Dor, Tuc-Hor, Argus, and the Hyades

Adam C. Schneider[1,4,5], James Windsor[2], Michael C. Cushing[2], J. Davy Kirkpatrick[3], and Evgenya L. Shkolnik[1]
[1] School of Earth and Space Exploration, Arizona State University, Tempe, AZ, 85282, USA; aschneid10@gmail.com
[2] Department of Physics and Astronomy, University of Toledo, 2801 W. Bancroft Street, Toledo, OH 43606, USA
[3] IPAC, Mail Code 100-22, Caltech, 1200 E. California Boulevard, Pasadena, CA 91125, USA
Received 2017 January 17; revised 2017 March 3; accepted 2017 March 10; published 2017 April 4

Abstract

Young brown dwarfs share many properties with directly imaged giant extrasolar planets. They therefore provide unique laboratories for investigating the full range of temperature and mass encompassed by the growing collection of planets discovered outside our Solar System. Furthermore, if they can be tied to a particular group of coeval stars, they also provide vital anchor points for low-mass empirical isochrones. We have developed a novel procedure for identifying such objects based on their unique 2MASS and AllWISE colors. Using our search criteria, we have identified 50 new, late-type L dwarf candidates, 47 of which are spectroscopically confirmed as L dwarfs with follow-up near-infrared spectroscopy. We evaluate the potential membership of these objects in nearby, young moving groups using their proper motions, photometric distance estimates, and spectroscopic indicators of youth, and find seven likely L-type members belonging to the β Pictoris moving group, the AB Doradus moving group, the Tucana-Horologium association, or the Argus association, in addition to several lower probability members. Also found are two late-type (L5 and L6) potential members of the nearby Hyades cluster (WISEA J043642.75+190134.8 and WISEA J044105.56+213001.5).

Key words: brown dwarfs

1. Introduction

Recent studies have shown that young, late-type brown dwarfs can be used as proxies for young, giant extrasolar planets (e.g., Faherty et al. 2016) because the same physics and chemistry governs the atmospheres of both sets of objects. Free-floating brown dwarfs are typically much easier to observe than their exoplanetary counterparts because they do not compete with the bright glare of a nearby host star. Furthermore, if a young brown dwarf can be tied to a nearby coeval moving group or cluster, it can serve as an evolutionary benchmark due to the fact that group properties, such as age and metallicity, can be applied to that object. Low-mass members are also critical for constraining the low-mass end of the initial mass function (IMF) of coeval nearby groups (e.g., Gagné et al. 2017).

Many of the young brown dwarfs in the literature have been found serendipitously through surveys for brown dwarfs or high proper motion objects (e.g., Kirkpatrick et al. 2006; Gizis et al. 2012; Liu et al. 2013; Mace et al. 2013; Thompson et al. 2013; Schneider et al. 2014; Kellogg et al. 2015). There are, however, recent efforts focused specifically on identifying young brown dwarfs (e.g., Gagné et al. 2015; Aller et al. 2016). These efforts typically use a combination of color criteria to select for late-type objects, and kinematic constraints associated with a particular association or associations to identify candidate moving group members. Such searches have been adept at identifying late-M to early-L bona fide and candidate members of nearby, young moving groups. These objects have ages ranging from $\sim$10 Myr to $\sim$150 Myr and, in some instances, have masses that extend into the planetary-mass regime (see Figure 34 of Faherty et al. 2016). Despite these targeted searches, the latest spectral type members ($\geqslant$L5) remain particularly elusive. The most likely reason for this is because such objects are much fainter than field age objects of the same spectral type, especially at the J passband (see Figure 15 of Liu et al. 2016). However, it is exactly these late-type members that make the most ideal proxies as exoplanet analogs and dictate the shape of the IMF at the low mass end.

One common trait among young, low-mass brown dwarfs is their red near- and mid-infrared colors compared to field age objects of the same spectral type (see, e.g., Figures 5–14 in Faherty et al. 2016). These red colors are typically ascribed to enhanced amounts of dust and/or clouds in their atmospheres, effectively shifting their emergent flux to longer wavelengths. The presence of excess clouds and dust is due to the lower surface gravities of these objects due to the fact that they are young and still contracting to their final radii. Note that, while red near-infrared colors are common among young brown dwarfs, there are examples of brown dwarfs with unusually red colors that are not believed to be young (e.g., Looper et al. 2008; Kirkpatrick et al. 2010; Marocco et al. 2014), and for some objects, alternative explanations have been proposed (e.g., disk structures—Zakhozhay et al. 2017). Nevertheless, we sought to identify more young, nearby, late-type brown dwarfs based on their uniquely red colors. We describe our search process in the following section, followed by a summary of our follow-up observations. Lastly, we present the results of the survey and discuss individual objects of note.

2. Identifying Young Late-type L Dwarfs

As noted in Schneider et al. (2014), young, late-type (>L5) brown dwarfs occupy a unique region of Two Micron All Sky

[4] Visiting Astronomer at the Infrared Telescope Facility, which is operated by the University of Hawaii under Cooperative Agreement no. NNX-08AE38A with the National Aeronautics and Space Administration, Science Mission Directorate, Planetary Astronomy Program.

[5] Visiting astronomer, Cerro Tololo Inter-American Observatory, National Optical Astronomy Observatory, which is operated by the Association of Universities for Research in Astronomy (AURA) under a cooperative agreement with the National Science Foundation.

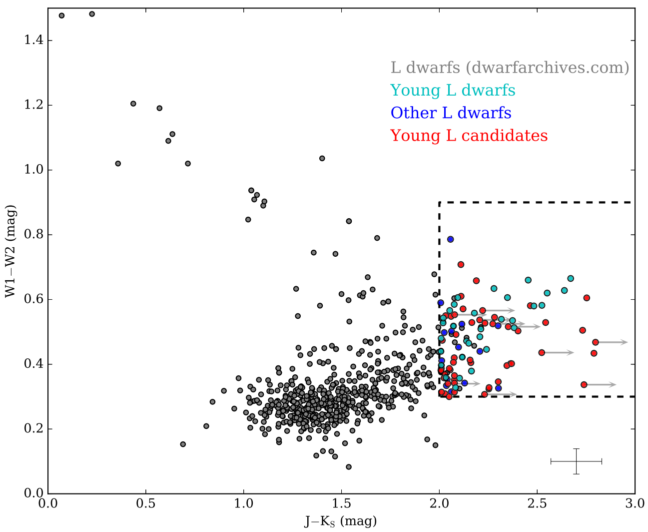

Figure 1. The $J - K_s$ vs. $W1-W2$ color–color diagram showing our young L candidates (red) along with recovered known L dwarfs from our search (young and otherwise—light and dark blue, respectively), and all L dwarfs from dwarfarchives.com (gray). The dashed black line indicates the search region of this survey. The typical photometric uncertainty for objects within our search region is plotted in the bottom right corner.

Survey (2MASS; Skrutskie et al. 2006) and *Wide-field Infrared Survey Explorer* (*WISE*; Wright et al. 2010) color space because they tend to have much redder colors than those of older field brown dwarfs, at least down to the L/T transition (Faherty et al. 2016; Liu et al. 2016). We investigated this region of color space for additional candidate young, late-type brown dwarfs. Specifically, we searched for objects within the 2MASS and AllWISE point source catalogs with $J - K_S \geqslant 2.0$ mag, $J - K_S \leqslant 3.5$ mag, $W1-W2 \geqslant 0.3$ mag, and $W1-W2 \leqslant 0.9$ mag (see Figure 1). This region was chosen to encompass known, red, young brown dwarfs, such as 2MASS J00470038+6803543 (Gizis et al. 2012), 2MASS J03552337+1133437 (Reid et al. 2006a), WISE J174102.78−464225.5 (Schneider et al. 2014), and 2MASS J22443167+2043433 (Dahn et al. 2002), as well as the young companion VHS 1256−1257b (Gauza et al. 2015), while excluding the majority of known L dwarfs, as shown in Figure 1. Note that we did not require objects to be detected in the *J*-band, anticipating the existence of objects so red in $J - K_S$ color that they may only be detected at the K_S-band.[6] We do, however, require that objects are well detected in the K_S, *W1*, and *W2* bands (i.e., not upper limits and photometric uncertainties $\leqslant$0.2 mag). We also avoid the galactic plane ($|b| > 5.0$ degrees) to exclude highly confused regions that would affect our 2MASS/AllWISE cross-match, and star-forming regions where the effects of reddening could be high, resulting in a significant increase of false positives. Lastly, we require that the separation between the 2MASS and AllWISE source positions be greater than $1''$, thereby ensuring each candidate shows appreciable proper motion between the 2MASS and AllWISE epochs ($\gtrsim$100 mas yr^{-1}, considering the ∼10 year time baseline between 2MASS and AllWISE). While there are certainly moving group members with total proper motion magnitudes <100 mas yr^{-1}, we chose this limit so that the motion of our candidates could be clearly seen in our finder chart inspection process (see next paragraph) and to return a reasonable number of candidates for inspection. These constraints returned 5555 sources.

We then scrutinized each candidate individually by creating and inspecting a finder chart for each source using available optical Digitized Sky Survey (DSS), near-infrared (2MASS), and mid-infrared (AllWISE) images (see, e.g., Schneider et al. 2016a) to ensure each candidate is a point source (i.e., not extended or blended) and has noticeable proper motion.

We found 98 young brown dwarf candidates with this search. Forty-eight of the candidates are previously known—47 are spectroscopically confirmed L dwarfs and 1 is WISEA J041847.95+252001.8, a highly reddened K dwarf (Kirkpatrick et al. 2016). Table 1 lists these 48 known objects, their discovery references, and their spectral types. Included in this list is the young L dwarf WISE 114724.10−204021.3 (Schneider et al. 2016b), the first discovery published from this survey. Of the 47 known L dwarfs, 25 are either known to be young or show some signs of youth in their spectra. This fraction (25/47, ∼53%) is much higher than the young L dwarf fraction of ∼8% reported by Kirkpatrick et al. (2008) in their analysis of field L dwarfs, showing the effectiveness of our method. The 2MASS and AllWISE photometry for the remaining 50 candidates are listed in Table 2. Note that some of these candidates have been identified as either high proper motion objects or brown dwarf candidates in the literature, but none have been spectroscopically confirmed. Previous references to these objects are noted in Section 4.2.

3. Observations

3.1. Infrared Telescope Facility (IRTF)/SpeX

Twenty-seven objects were observed using the SpeX spectrograph (Rayner et al. 2003) at NASA's 3 m IRTF. All observations were made in prism mode with a $0\farcs5$-wide slit, resulting in a resolving power ($\lambda/\Delta\lambda$) of ∼150 over the 0.8–2.5 μm range. For each observation, the slit was oriented along the parallactic angle and exposures were taken at two different nod positions. A0V stars at similar airmasses were observed immediately after each science target for telluric correction purposes. Each spectrum was reduced using the SpeXtool reduction package (Vacca et al. 2003; Cushing et al. 2004). A summary of all IRTF/SpeX observations, including observation dates and exposure times, is given in Table 3.

3.2. Magellan/FIRE

Nine objects were observed with the Folded-port Infrared Echellette (FIRE; Simcoe et al. 2013) spectrograph located at the 6.5 m Baade *Magellan* telescope. All observations were made with the high-throughput prism mode, which achieved a resolving power of ∼450 across the 0.8–2.45 μm range. We used the $0\farcs6$ slit, aligned to the parallactic angle, and took exposures at two different nod positions along the slit. For all science targets, we used the sample-up-the-ramp mode. A0V stars were observed after each science target to correct for telluric absorption. All reductions were performed using a modified version of the SpeXtool reduction package (Vacca et al. 2003; Cushing et al. 2004). A summary of all *Magellan*/FIRE observations, including observation dates and exposure times, is given in Table 3.

[6] Note that in cases where *J* band magnitudes are upper limits, such objects may have $J - K_S$ colors redder than 3.5 mag.

Table 1
Known Brown Dwarfs Recovered in This Survey

AllWISE Designation	Other Name	Disc. References	Sp. Type	Sp. Type References	Young?[a]
J000627.85+185728.8	...	Schneider et al. (2016a)	L7	Schneider et al. (2016a)	N
J001851.52+515330.6	PSO J004.7148+51.8918	Best et al. (2015)	L7	Best et al. (2015)	Y?
J004701.09+680352.2	2MASS J00470038+6803543	Gizis et al. (2012)	L7 INT-G	Gizis et al. (2015)	Y
J010332.31+193536.3	2MASSI J0103320+193536	Kirkpatrick et al. (2000)	L6β	Faherty et al. (2012)	Y
J010752.84+004157.1	2MASS J01075242+0041563	Geballe et al. (2002)	L7 pec	Gagné et al. (2015)	N
J012912.40+351757.3	2MASSW J0129122+351758	Kirkpatrick et al. (1999)	L4	Kirkpatrick et al. (1999)	Y?
J020503.72+125142.0	2MASSI J0205034+125142	Kirkpatrick et al. (2000)	L6.5	Schneider et al. (2014)	N
J020625.28+264023.5	WISEPA J020625.26+264023.6	Kirkpatrick et al. (2011)	L9 pec (red)	Kirkpatrick et al. (2011)	N?
J031854.39−342128.7	2MASS J03185403−3421292	Cruz et al. (2007)	L7	Schneider et al. (2014)	N
J032642.33−210207.3	2MASS J03264225−2102057	Gizis et al. (2003)	L5 β/γ	Gagné et al. (2015)	Y
J033703.75−175806.5	2MASS J03370359−1758079	Kirkpatrick et al. (2000)	L4.5	Kirkpatrick et al. (2000)	N
J034909.45+151436.0	PSO J057.2893+15.2433	Best et al. (2015)	L7 red	Best et al. (2015)	Y?
J035523.53+113337.2	2MASS J03552337+1133437	Reid et al. (2006a)	L5γ	Faherty et al. (2013)	Y
J035822.61−411604.9	2MASS J03582255−4116060	Reid et al. (2008)	L6 pec	Gagné et al. (2015)	Y?
J040057.53−132204.2	SIMP J04005763−1322024	Robert et al. (2016)	L7::	Robert et al. (2016)	N
J041847.95+252001.8	...	Kirkpatrick et al. (2016)	~K (reddened)	Kirkpatrick et al. (2016)	N
J042107.45−630559.7	2MASS J04210718−6306022	Cruz et al. (2007)	L5γ	Faherty et al. (2013)	Y
J044635.41+145125.8	2MASS J04463535+1451261	Hogan et al. (2008)	L2	Lodieu et al. (2014)	Y
J050124.21−001047.1	2MASS J05012406−0010452	Reid et al. (2008)	L3 VL-G	Allers & Liu (2013)	Y
J074006.95+200920.0	SDSS J074007.30+200921.9	Knapp et al. (2004)	L6	Chiu et al. (2006)	N
J080958.86+443419.4	SDSS J080959.01+443422.2	Knapp et al. (2004)	L6 pec (red)	Gagné et al. (2015)	Y?
J082029.81+450027.7	2MASS J08202996+4500315	Kirkpatrick et al. (2000)	L7	Schneider et al. (2014)	N
J082519.23+211548.3	2MASS J08251968+2115521	Kirkpatrick et al. (2000)	L7 pec	Gagné et al. (2015)	Y?
J082957.00+265509.2	2MASSW J0829570+265510	Kirkpatrick et al. (2000)	L6.5	Kirkpatrick et al. (2000)	Y?
J083542.14−081920.1	2MASS J08354256−0819237	Cruz et al. (2003)	L4 pec	Gagné et al. (2015)	Y?
J085757.94+570847.3	2MASS J08575849+5708514	Geballe et al. (2002)	L8 pec	Gagné et al. (2015)	Y?
J095533.26−020841.6	2MASS J09553336−0208403	Gagné et al. (2017)	L7 red	Gagné et al. (2017)	Y
J095608.17−144708.2	PSO J149.0341−14.7857	Best et al. (2015)	L9	Best et al. (2015)	N
J095932.66+452329.3	2MASS J09593276+4523309	Zhang et al. (2009)	L7.5	Zhang et al. (2009)	Y
J100420.50+502257.6	G 196−3B	Rebolo et al. (1998)	L2-L4γ	Gagné et al. (2015)	Y
J110233.55−235945.6	2MASS J11023375−2359464	Kirkpatrick et al. (2000)	L4.5	Kirkpatrick et al. (2000)	N
J111932.43−113747.7	2MASS J11193254−1137466	Kellogg et al. (2015)	L7 red	Kellogg et al. (2016)	Y
J114724.10−204021.3	...	Schneider et al. (2016b)	L7γ	Schneider et al. (2016b)	Y
J125601.66−125728.7	VHS 1256−1257b	Gauza et al. (2015)	L8	Gauza et al. (2015)	Y
J130729.56−055815.4	...	Schneider et al. (2016a)	L8 (sl. blue)	Schneider et al. (2016a)	N
J134316.31+394509.9	2MASSI J1343167+394508	Kirkpatrick et al. (2000)	L5	Kirkpatrick et al. (2000)	N
J155152.32+094114.2	2MASS J15515237+0941148	Reid et al. (2008)	L4γ	Faherty et al. (2013)	Y
J155321.37+210908.4	2MASSW J1553214+210907	Kirkpatrick et al. (1999)	L5.5	Kirkpatrick et al. (1999)	N
J161542.44+495321.3	2MASS J16154255+4953211	Metchev et al. (2008)	L3−L6γ	Gagné et al. (2015)	Y
J164715.57+563208.3	WISEPA J164715.59+563208.2	Kirkpatrick et al. (2011)	L9 pec (red)	Kirkpatrick et al. (2011)	N?
J172600.03+153818.2	2MASSI J1726000+153819	Kirkpatrick et al. (2000)	L3β	Cruz et al. (2009)	Y
J174102.77−464225.7	WISE J174102.78−464225.5	Schneider et al. (2014)	L5:−L7:γ	Gagné et al. (2015)	Y
J205202.06−204313.0	...	Schneider et al. (2016a)	L8 (sl. blue)	Schneider et al. (2016a)	N
J214817.01+400404.1	2MASS J21481628+4003593	Looper et al. (2008)	L6 (red)	Schneider et al. (2014)	N?
J215125.68−244100.5	2MASSI J2151254−244100	Liebert & Gizis (2006)	L4 pec	Gagné et al. (2015)	Y?
J215434.68−105530.8	SIMP J215434.5−105530.8	Gagné et al. (2014a)	L5β/γ	Gagné et al. (2015)	Y
J224431.89+204340.2	2MASS J22443167+2043433	Dahn et al. (2002)	L6−L8γ	Gagné et al. (2015)	Y
J234334.79−364603.4	2MASS J23433470−3646021	Gagné et al. (2015)	L3−L6γ	Gagné et al. (2015)	Y

Note.
[a] Previously determined signs of youth, where "Y"—young, "Y?"—likely young, "N"—not young, and, "N?"—unlikely to be young.

3.3. CTIO Blanco 4 m/ARCoIRIS

Twenty-two objects were observed with the Astronomy Research using the Cornell Infrared Imaging Spectrograph (ARCoIRIS) on the 4 m Blanco telescope located at the Cerro Tololo Inter-American Observatory (CTIO). ARCoIRIS takes simultaneous spectra across six cross-dispersed orders covering the 0.8–2.4 μm range, with a resolving power of ~3500. Science exposures were taken at two different nod positions along the slit, which has a fixed width of 1$''$.1. After each science target, A0V stars were observed in order to execute telluric corrections. Reductions were performed using a modified version of the SpeXtool reduction package (Vacca et al. 2003; Cushing et al. 2004). A summary of all ARCoIRIS observations, including observation dates and exposure times, is given in Table 3.

4. Analysis

4.1. Basic Properties of the Entire Sample

A total of 50 L-type brown dwarf candidates were found with this survey, 47 of which we have observed

Table 2
2MASS and AllWISE Photometry of New Discoveries

AllWISE Designation	J (mag)	H (mag)	K_S (mag)	$W1$ (mag)	$W2$ (mag)
J002050.25−151913.1	16.962 ± 0.151	15.622 ± 0.102	14.933 ± 0.112	14.360 ± 0.030	14.051 ± 0.047
J003052.08−380829.6	17.180 ± 0.231	16.062 ± 0.175	15.172 ± 0.162	14.898 ± 0.032	14.516 ± 0.051
J004403.39+022810.6	16.997 ± 0.187	15.822 ± 0.169	14.876 ± 0.104	14.016 ± 0.027	13.445 ± 0.036
J005811.69−565332.1	16.778 ± 0.165	15.554 ± 0.135	14.545 ± 0.094	13.763 ± 0.025	13.236 ± 0.028
J010738.75−131413.7	16.710 ± 0.131	15.577 ± 0.120	14.625 ± 0.095	13.934 ± 0.027	13.442 ± 0.032
J013556.99−620245.5	17.395 ± 0.271	16.187 ± 0.217	15.094 ± 0.138	14.793 ± 0.029	14.447 ± 0.041
J014535.23−031412.9	17.124 ± 0.182	15.810 ± 0.140	14.958 ± 0.110	14.150 ± 0.027	13.621 ± 0.035
J020047.29−510521.4	16.414 ± 0.124	14.941 ± 0.069	13.871 ± 0.052	12.885 ± 0.024	12.356 ± 0.023
J020229.29+230513.9	17.221 ± 0.230	15.858 ± 0.129	15.206 ± 0.146	14.241 ± 0.027	13.767 ± 0.035
J022609.16−161000.4	17.334 ± 0.266	15.750 ± 0.142	14.581 ± 0.093	13.745 ± 0.025	13.140 ± 0.027
J023749.81−260543.8	16.777 ± 0.172	15.610 ± 0.135	14.768 ± 0.121	14.229 ± 0.026	13.848 ± 0.032
J025954.88−314655.6	17.487 ± 0.239	16.380 ± 0.184	15.437 ± 0.169	14.919 ± 0.030	14.619 ± 0.047
J032049.31−532656.7	17.032 ± 0.225	15.664 ± 0.128	14.871 ± 0.129	14.162 ± 0.026	13.757 ± 0.029
J032440.23−191905.6	17.007 ± 0.205	15.591 ± 0.154	14.605 ± 0.111	14.125 ± 0.027	13.622 ± 0.031
J041232.77+104408.3	17.606 ± 0.255	16.144 ± 0.164	15.242 ± 0.113	14.270 ± 0.029	13.868 ± 0.040
J042231.34+081012.7	17.272 ± 0.226	>16.043	15.240 ± 0.135	15.618 ± 0.050	15.068 ± 0.095
J042506.66−425509.6	16.616 ± 0.135	15.011 ± 0.060	14.427 ± 0.067	13.477 ± 0.024	12.819 ± 0.024
J043642.75+190134.8	17.121 ± 0.175	15.657 ± 0.098	14.868 ± 0.094	14.193 ± 0.030	13.869 ± 0.043
J043718.77−550944.0	16.985 ± 0.192	15.583 ± 0.157	14.640 ± 0.098	14.135 ± 0.024	13.739 ± 0.026
J044105.56+213001.5	17.274 ± 0.218	16.141 ± 0.168	15.197 ± 0.130	14.554 ± 0.032	14.202 ± 0.052
J045900.42−285338.3	17.429 ± 0.282	16.375 ± 0.249	15.318 ± 0.197	14.305 ± 0.026	13.695 ± 0.028
J050259.73−610206.1	17.087 ± 0.187	15.945 ± 0.149	15.010 ± 0.151	14.698 ± 0.026	14.356 ± 0.033
J055959.30−583546.0	16.686 ± 0.144	15.416 ± 0.097	14.631 ± 0.090	14.450 ± 0.026	14.067 ± 0.032
J065935.80+771457.8	16.865 ± 0.171	15.594 ± 0.115	14.708 ± 0.096	14.215 ± 0.026	13.802 ± 0.033
J070534.00−183925.6	16.778 ± 0.129	15.498 ± 0.092	14.701 ± 0.092	13.977 ± 0.028	13.612 ± 0.035
J071138.88+370601.0	17.165 ± 0.243	15.466 ± 0.131	14.911 ± 0.094	14.414 ± 0.030	14.086 ± 0.053
J072352.62−330943.5	15.743 ± 0.059	14.471 ± 0.043	13.715 ± 0.047	13.068 ± 0.023	12.699 ± 0.023
J081322.19−152203.2	>17.658	16.252 ± 0.183	14.860 ± 0.126	13.984 ± 0.026	13.516 ± 0.030
J082624.09−601202.8	>17.559	16.133 ± 0.205	14.820 ± 0.126	14.517 ± 0.026	14.180 ± 0.033
J090258.99+670833.1	16.979 ± 0.246	15.089 ± 0.106	14.247 ± 0.108	13.200 ± 0.025	12.695 ± 0.026
J093858.10+761211.5	16.984 ± 0.181	15.595 ± 0.124	14.908 ± 0.106	14.275 ± 0.026	13.855 ± 0.034
J120104.57+573004.2	17.355 ± 0.235	16.407 ± 0.266	15.245 ± 0.133	14.368 ± 0.028	13.660 ± 0.032
J130523.06−395104.9	>17.107	16.138 ± 0.224	15.029 ± 0.133	14.193 ± 0.027	13.640 ± 0.032
J131845.58+362614.0	17.212 ± 0.209	15.844 ± 0.136	15.161 ± 0.117	14.538 ± 0.028	14.151 ± 0.041
J143211.17+324433.8	>17.359	16.081 ± 0.186	15.138 ± 0.126	14.300 ± 0.027	13.734 ± 0.030
J145642.68+645009.7	17.564 ± 0.310	15.631 ± 0.115	14.774 ± 0.102	13.888 ± 0.025	13.454 ± 0.027
J153358.52+475706.9	>17.280	15.909 ± 0.152	14.928 ± 0.152	14.374 ± 0.025	13.858 ± 0.031
J162341.27−740230.4	>17.075	15.481 ± 0.147	14.869 ± 0.131	13.923 ± 0.027	13.386 ± 0.030
J173453.90−481357.9	16.285 ± 0.127	14.865 ± 0.075	13.916 ± 0.052	12.968 ± 0.025	12.566 ± 0.026
J174057.82+131709.4	>17.468	16.257 ± 0.212	15.195 ± 0.149	14.764 ± 0.033	14.239 ± 0.046
J190722.56+472745.3	16.402 ± 0.124	15.269 ± 0.110	14.330 ± 0.073	13.862 ± 0.024	13.456 ± 0.027
J201204.11+672608.0	17.148 ± 0.239	15.850 ± 0.179	15.124 ± 0.137	14.336 ± 0.025	13.978 ± 0.030
J201530.67−421542.5	17.648 ± 0.317	16.233 ± 0.151	15.366 ± 0.145	14.592 ± 0.030	14.047 ± 0.041
J201826.00−332207.3	>17.33	15.908 ± 0.210	15.286 ± 0.147	15.153 ± 0.038	14.813 ± 0.073
J204902.80−745613.5	>17.789	16.328 ± 0.229	15.266 ± 0.163	14.595 ± 0.028	14.159 ± 0.035
J225333.00−253948.0	17.152 ± 0.214	15.752 ± 0.148	15.075 ± 0.144	14.544 ± 0.029	14.230 ± 0.047
J232307.08+054113.0	17.600 ± 0.276	15.961 ± 0.165	15.540 ± 0.173	14.642 ± 0.032	14.094 ± 0.043
J232453.73+503525.4	>17.084	15.868 ± 0.181	14.853 ± 0.104	14.449 ± 0.027	14.142 ± 0.035
J233333.46+025128.4	16.688 ± 0.127	15.407 ± 0.093	14.677 ± 0.086	14.158 ± 0.028	13.844 ± 0.042
J235422.31−081129.7	17.255 ± 0.230	15.962 ± 0.150	14.790 ± 0.119	13.962 ± 0.027	13.381 ± 0.033

spectroscopically and confirm as L dwarfs. We determine spectral types for all near-infrared spectra following the method outlined in the Appendix of Schneider et al. (2014), whereby we compare each spectrum via a χ^2 fit to every near-infrared L dwarf spectral standard from Kirkpatrick et al. (2010) normalized between 1.27 and 1.29 μm. Each spectrum is then inspected by eye to find the best fit, with the results of the χ^2 fitting as a guide. The uncertainties after the by-eye inspection are ±0.5 subtypes, except in cases of low signal-to-noise (S/N < 10), where we assume a ±1 subtype uncertainty. All spectral types are given in Table 4, and comparisons of each acquired spectrum with the corresponding near-infrared spectral standards from the Spex Prism Spectral Library[7] are shown in Figures 2–5. If more than one spectrum was obtained for an object, the spectrum shown is that with the higher S/N. For the 10 objects for which we have multiple spectra, all spectral types were consistent between observations. Any ARCoIRIS spectrum shown has been smoothed to a similar resolution to the near-infrared spectral standards for comparison.

[7] http://pono.ucsd.edu/ãdam/browndwarfs/spexprism/library.html

Table 3
Summary of Observations

AllWISE Designation	Telescope/ Instrument	Obs. Date (UT)	Exp. Time (s)	S/N$_J$[a]
J002050.25−151913.1	CTIO/ARCoIRIS	2016 Dec 10	1440	3
J003052.08−380829.6	*Magellan*/FIRE	2016 Jul 18	1014	29
J003052.08−380829.6	CTIO/ARCoIRIS	2016 Aug 22	2160	11
J004403.39+022810.6	IRTF/SpeX	2016 Sep 29	2160	20
J005811.69−565332.1	*Magellan*/FIRE	2016 Jul 17	1014	26
J005811.69−565332.1	CTIO/ARCoIRIS	2016 Aug 19	2160	5
J010738.75−131413.7	IRTF/SpeX	2016 Sep 30	2640	6
J013556.99−620245.5	*Magellan*/FIRE	2016 Jul 17	1014	19
J013556.99−620245.5	CTIO/ARCoIRIS	2016 Aug 22	2160	8
J014535.23−031412.9	IRTF/SpeX	2016 Sep 29	1440	19
J020047.29−510521.4	*Magellan*/FIRE	2016 Jul 17	761	55
J020047.29−510521.4	CTIO/ARCoIRIS	2016 Aug 22	960	15
J020229.29+230513.9	IRTF/SpeX	2016 Sep 28	2160	24
J022609.16−161000.4	*Magellan*/FIRE	2016 Jul 18	1014	22
J022609.16−161000.4	IRTF/SpeX	2016 Sep 29	2160	17
J023749.81−260543.8	CTIO/ARCoIRIS	2016 Dec 11	2160	10
J025954.88−314655.6	CTIO/ARCoIRIS	2016 Dec 10	2160	8
J032049.31−532656.7	CTIO/ARCoIRIS	2016 Dec 11	2160	11
J032440.23−191905.6	IRTF/SpeX	2016 Sep 28	2160	36
J041232.77+104408.3	IRTF/SpeX	2016 Sep 30	2880	12
J042231.34+081012.7	IRTF/SpeX	2016 Sep 29	2160	17
J042506.66−425509.6	CTIO/ARCoIRIS	2016 Jan 25	2040	12
J043642.75+190134.8	IRTF/SpeX	2016 Feb 12	1440	12
J043718.77−550944.0	CTIO/ARCoIRIS	2016 Dec 11	2160	10
J044105.56+213001.5	IRTF/SpeX	2016 Sep 28	2880	10
J045900.42−285338.3	CTIO/ARCoIRIS	2016 Dec 10	2160	4
J050259.73−610206.1	CTIO/ARCoIRIS	2016 Dec 9	2160	5
J055959.30−583546.0	CTIO/ARCoIRIS	2016 Dec 10	2160	11
J070534.00−183925.6	IRTF/SpeX	2016 Feb 12	1440	18
J071138.88+370601.0	IRTF/SpeX	2016 Feb 12	1440	22
J072352.62−330943.5	IRTF/SpeX	2016 Feb 12	1440	53
J081322.19−152203.2	CTIO/ARCoIRIS	2016 Dec 11	2160	8
J082624.09−601202.8	CTIO/ARCoIRIS	2016 Dec 11	2160	10
J090258.99+670833.1	IRTF/SpeX	2016 Feb 12	2160	56
J095533.26−020841.6	IRTF/SpeX	2016 Feb 12	2160	17
J120104.57+573004.2	IRTF/SpeX	2016 Feb 12	2160	22
J130523.06−395104.9	IRTF/SpeX	2016 Feb 12	1440	7
J131845.58+362614.0	IRTF/SpeX	2016 Feb 12	1440	30
J143211.17+324433.8	IRTF/SpeX	2016 May 31	2160	16
J145642.68+645009.7	IRTF/SpeX	2016 Feb 12	1920	31
J153358.52+475706.9	IRTF/SpeX	2016 May 31	2160	16
J162341.27−740230.4	*Magellan*/FIRE	2016 Jul 17	1268	42
J162341.27−740230.4	CTIO/ARCoIRIS	2016 Aug 22	2160	6
J173453.90−481357.9	CTIO/ARCoIRIS	2016 Aug 19	1440	10
J174057.82+131709.4	IRTF/SpeX	2016 May 31	1440	17
J190722.56+472745.3	IRTF/SpeX	2016 Jun 26	2160	39
J201204.11+672608.0	IRTF/SpeX	2016 Jun 26	2160	8
J201530.67−421542.5	CTIO/ARCoIRIS	2016 Jun 21	1440	8
J201826.00−332207.3	*Magellan*/FIRE	2016 Jul 17	1268	34
J201826.00−332207.3	CTIO/ARCoIRIS	2016 Aug 22	2160	10
J204902.80−745613.5	CTIO/ARCoIRIS	2016 Jun 22	2880	6
J225333.00−253948.0	*Magellan*/FIRE	2016 Jul 18	1014	38
J225333.00−253948.0	CTIO/ARCoIRIS	2016 Aug 19	2160	5
J232307.08+054113.0	*Magellan*/FIRE	2016 Jul 18	1014	11
J232307.08+054113.0	IRTF/SpeX	2016 Sep 29	2160	19
J233333.46+025128.4	IRTF/SpeX	2016 Sep 28	1440	29
J235422.31−081129.7	IRTF/SpeX	2016 Sep 29	2160	21
J235422.31−081129.7	CTIO/ARCoIRIS	2016 Aug 22	2160	7

Note.
[a] Signal-to-noise ratio achieved between 1.27 and 1.29 μm.

We calculate the proper motion of each object using the positions from the AllWISE and 2MASS source catalogs. Proper motion uncertainties are determined from the positional uncertainties for each object provided in the AllWISE and 2MASS catalogs. Proper motions and uncertainties are given in Table 4.

As discussed in Schneider et al. (2016b) (see also Faherty et al. 2013), the photometric distances of young, late-type L dwarfs closely match their measured parallactic distances using K-band magnitudes. While not all objects in this sample are young, we find that several are likely members of nearby moving groups (see Section 5). We therefore calculate photometric distances using the 2MASS K_S-band magnitude and the absolute magnitude-spectral type relations from Dupuy & Liu (2012). The photometric distance uncertainties include both spectral type and photometric uncertainties. Two recent, extensive parallax programs focused on young brown dwarfs (Faherty et al. 2016 and Liu et al. 2016) allow us to investigate if this K-band assumption holds true for a much larger sample of low gravity objects than that investigated in Schneider et al. (2016b). If the difference between photometric K-band estimates and actual measured parallaxes is small for young brown dwarfs, then there should be little difference between the absolute magnitudes of young L dwarfs and field L dwarfs per spectral type bin when using K-band photometry. Indeed this is the case in both studies (see Figure 17 of Faherty et al. 2016 and Figure 6 of Liu et al. 2016). All photometric distance estimates for the new discoveries presented here are given in Table 4. We assume each object is single for these estimates.

4.2. Sample Comparison

We first inspect all objects recovered with this survey as a whole. The left panel of Figure 6 shows a color–color diagram comparing the positions of four distinct samples recovered in this survey; known young L dwarfs ("Y" or "Y?" in Table 1), known L dwarfs without any mention of youth in the literature, new discoveries from this survey with "red" or "sl. red" spectral types, and the remainder of the discoveries from this survey. The known young L dwarfs and new "red" discoveries generally occupy the same region of color space. While the new discoveries not labeled as "red" extend over much of the same color space as known young Ls and the new "red" discoveries, there is a significantly larger population of these objects at the bluest corner of this color space. This is not unexpected, as the vast majority of these objects are expected to have ages consistent with the field population.

We also compare the same sets of objects on a reduced proper motion diagram to investigate whether these populations show kinematically distinct characteristics. The reduced proper motion is defined as $H_m = m + 5\log(\mu) + 5$, where m is a particular photometric band and μ is the object's total proper motion. We chose to use the 2MASS K_S magnitude for this diagram as some objects have upper limits in the 2MASS J band. Again, the new "red" discoveries and the known young L dwarfs generally occupy the same regions of this diagram. While there is some overlap, these two groups look to be kinematically distinct from both the other known L dwarfs and discoveries not found to be "red." In general, the new "red" discoveries and known young L dwarfs tend to be redder and have smaller reduced proper motion magnitudes. While 17 of the 47 known young or new "red" objects have reduced proper motion magnitudes greater than 16 (∼36%), a significantly larger fraction of the remaining objects have reduced proper motion magnitudes greater than 16 (30/50, or 60%).

4.3. Previously Proposed Brown Dwarf Candidates

We provide the first spectra of several objects which have been identified previously as brown dwarf candidates in the literature.

4.3.1. WISEA J004403.39+022810.6, WISEA J232307.08+054113.0, and WISEA J233333.46+025128.4

All three of these objects were identified as a brown dwarf candidates in Skrzypek et al. (2016). Skrzypek et al. (2016) classified these objects using photometry alone and found L7p, L8.5, and L4.5 for WISEA J004403.39+022810.6, WISEA J232307.08+054113.0, and WISEA J233333.46+025128.4, respectively. We find similar spectral types from our spectra in all three instances; L7 (sl. red) for WISEA J004403.39+022810.6, L8 (sl. blue) for WISEA J232307.08+054113.0, and L6 for WISEA J233333.46+025128.4. See additional discussion of the potential youth and moving group membership of WISEA J004403.39+022810.6 in Section 5.1.1.

4.3.2. WISEA J005811.69−565332.1 and WISEA J020047.29−510521.4

These objects were identified as a potential moving group members in Gagné et al. (2015), where WISEA J005811.69−565332.1 was found to be a modest probability Argus member and WISEA J020047.29−510521.4 was identified as a high probability (∼99%) member of ABDor. We present the first spectroscopic confirmation of these objects as L dwarfs in Figures 4 and 5 and determine a spectral types of L7 (sl. red) and L9 (red) for WISEA J005811.69−565332.1 and WISEA J020047.29−510521.4, respectively. Additional discussion of the potential youth and moving group membership of these objects is provided in Sections 5.1.2 and 5.1.3.

4.3.3. WISEA J162341.27−740230.4 and WISEA J201204.11+672608.0

These objects were previously identified as high proper motion objects in Luhman (2014). We present the first spectrum of these objects in Figures 4 and 5 and determine spectral types of L9 (sl. red) and L7: for WISEA J162341.27−740230.4 and WISEA J201204.11+672608.0, respectively. See additional discussion of the potential youth and moving group membership of WISEA J162341.27−740230.4 in Section 5.1.17.

5. Potentially Young Objects

A significant portion of our new discoveries show redder spectral slopes compared to their corresponding near-infrared spectral standards, and are labeled as "red" or "sl. red" in Table 4. For these potentially young objects (20 in total), we investigate whether or not they belong to any young, nearby, moving groups with three different available algorithms; BANYAN II (Malo et al. 2013; Gagné et al. 2014b), LACEwING (Riedel et al. 2017), and the Convergent Point ("CP") method from Rodriguez et al. (2013). For BANYAN II and LACEwING, we use the "young" option for all objects.

The BANYAN II moving group membership evaluation tool uses a naive Bayesian classifier analysis to assess membership

Table 4
Derived Properties of New Discoveries

AllWISE Designation	Sp. Type	μ_α (mas yr^{-1})	μ_δ (mas yr^{-1})	d_{phot}[a] (pc)
J002050.25−151913.1	L6:	158.5 ± 15.9	−13.6 ± 14.9	36 ± 6
J003052.08−380829.6	L5	150.1 ± 26.1	−33.4 ± 24.4	45 ± 6
J004403.39+022810.6	L7 (sl. red)	104.8 ± 15.4	−61.9 ± 14.5	31 ± 3
J005811.69−565332.1	L9 (red)	197.4 ± 12.8	46.0 ± 11.9	22 ± 2
J010738.75−131413.7	L7:	101.3 ± 11.6	−25.1 ± 10.8	28 ± 5
J013556.99−620245.5	L4	180.6 ± 29.4	91.5 ± 27.6	49 ± 7
J014535.23−031412.9	L9	29.5 ± 14.9	−97.4 ± 14.9	27 ± 3
J020047.29−510521.4	L7 (red)	171.2 ± 9.9	−75.4 ± 8.2	20 ± 2
J020229.29+230513.9	L7	128.6 ± 24.7	−15.4 ± 24.7	36 ± 5
J022609.16−161000.4	L7 (red)	100.3 ± 11.5	−108.5 ± 9.9	27 ± 3
J023749.81−260543.8	L2 (red)	−71.0 ± 13.5	−55.8 ± 11.1	56 ± 8
J025954.88−314655.6	L4:	−227.6 ± 24.0	−179.7 ± 24.0	57 ± 13
J032049.31−532656.7	L6	80.8 ± 16.2	−166.8 ± 14.4	35 ± 4
J032440.23−191905.6	L8 (blue)	−118.4 ± 12.9	−213.3 ± 12.0	25 ± 3
J041232.77+104408.3	L5: (red)	114.3 ± 30.3	52.5 ± 29.4	46 ± 6
J042231.34+081012.7	L1	−115.7 ± 29.7	−102.0 ± 28.1	80 ± 12
J042506.66−425509.6	L8	−133.9 ± 8.6	−100.4 ± 8.6	23 ± 2
J043642.75+190134.8	L6	98.8 ± 16.5	−29.0 ± 12.5	35 ± 4
J043718.77−550944.0	L5 (red)	76.2 ± 12.9	91.4 ± 12.0	35 ± 7
J044105.56+213001.5	L5 (sl. red)	98.1 ± 27.3	−39.0 ± 23.2	45 ± 9
J045900.42−285338.3	L7: (red)	85.3 ± 34.4	110.3 ± 30.9	38 ± 8
J050259.73−610206.1	L4:	35.2 ± 22.6	−253.3 ± 20.1	47 ± 11
J055959.30−583546.0	L2	−52.0 ± 9.9	−99.8 ± 9.1	52 ± 6
J065935.80+771457.8	…	7.9 ± 13.2	−146.2 ± 12.4	…
J070534.00−183925.6	L8	−243.2 ± 12.4	112.7 ± 11.0	26 ± 2
J071138.88+370601.0	L6	−73.7 ± 11.9	−287.3 ± 11.2	35 ± 4
J072352.62−330943.5	L5 (sl. red)	−37.3 ± 6.4	101.1 ± 6.4	23 ± 2
J081322.19−152203.2	L7: (sl. red)	−164.5 ± 14.7	98.8 ± 13.8	31 ± 6
J082624.09−601202.8	L8	−156.9 ± 16.6	−234.2 ± 14.0	28 ± 3
J090258.99+670833.1	L7 (sl. red)	−112.7 ± 10.6	−213.2 ± 9.8	23 ± 2
J093858.10+761211.5	…	−12.6 ± 15.4	104.2 ± 14.6	…
J120104.57+573004.2	L9	98.6 ± 28.9	13.0 ± 25.6	30 ± 3
J130523.06−395104.9	L8: (red)	−241.7 ± 15.8	−49.4 ± 15.8	30 ± 5
J131845.58+362614.0	L6 (sl. red)	−88.2 ± 23.1	23.4 ± 20.0	40 ± 5
J143211.17+324433.8	L7	−116.5 ± 25.5	1.8 ± 24.6	35 ± 4
J145642.68+645009.7	L7 (sl. red)	−198.8 ± 13.3	54.8 ± 12.4	30 ± 3
J153358.52+475706.9	L8:	−135.8 ± 20.9	35.0 ± 20.9	29 ± 4
J162341.27−740230.4	L9 (sl. red)	−122.6 ± 16.8	−378.7 ± 14.0	26 ± 3
J173453.90−481357.9	L5 (red)	−100.6 ± 9.3	−228.5 ± 9.2	25 ± 2
J174057.82+131709.4	L9	−17.5 ± 21.5	−220.4 ± 21.6	30 ± 4
J190722.56+472745.3	L6	40.1 ± 8.4	−89.6 ± 8.3	27 ± 3
J201204.11+672608.0	L7:	186.1 ± 25.2	216.9 ± 24.3	35 ± 6
J201530.67−421542.5	L7:	76.5 ± 35.1	−55.1 ± 33.3	39 ± 7
J201826.00−332207.3	L3	26.6 ± 22.1	−186.8 ± 21.3	61 ± 9
J204902.80−745613.5	L7: (red)	45.9 ± 29.5	−120.8 ± 27.5	37 ± 5
J225333.00−253948.0	L5	145.9 ± 23.1	−40.7 ± 20.6	43 ± 6
J232307.08+054113.0	L8 (sl. blue)	−179.8 ± 32.7	−112.8 ± 30.7	38 ± 5
J232453.73+503525.4	…	182.0 ± 11.3	58.2 ± 11.2	…
J233333.46+025128.4	L6 (sl. blue)	272.7 ± 14.4	169.9 ± 10.1	32 ± 3
J235422.31−081129.7	L5 (red)	130.1 ± 14.2	−70.1 ± 12.6	38 ± 5

Note.
[a] Photometric distance using the 2MASS K_S magnitude and the absolute magnitude-spectral type relations from Dupuy & Liu (2012).

probabilities for several nearby, young moving groups, including the AB Doradus moving group (AB Dor), Argus, the β Pictoris moving group (β Pic), Carina, Columba, Tucana-Horologium (Tuc-Hor), and the TW Hydra association (TWA). For each suspected young object in our sample, we use its proper motion and AllWISE position to determine potential membership probabilities. In Table 5, we report all membership probabilities greater than 10% found with BANYAN II. We also report the predicted distances given by BANYAN II assuming an object is a moving group member. This sample includes both moving group members and "Young field" objects. Note that Liu et al. (2016) find that the kinematic distances from BANYAN II agree to within 2.3σ with measured parallax distances for 90% of the objects they compared. In almost all cases where photometric and predicted distances disagree, the predicted distance is significantly closer

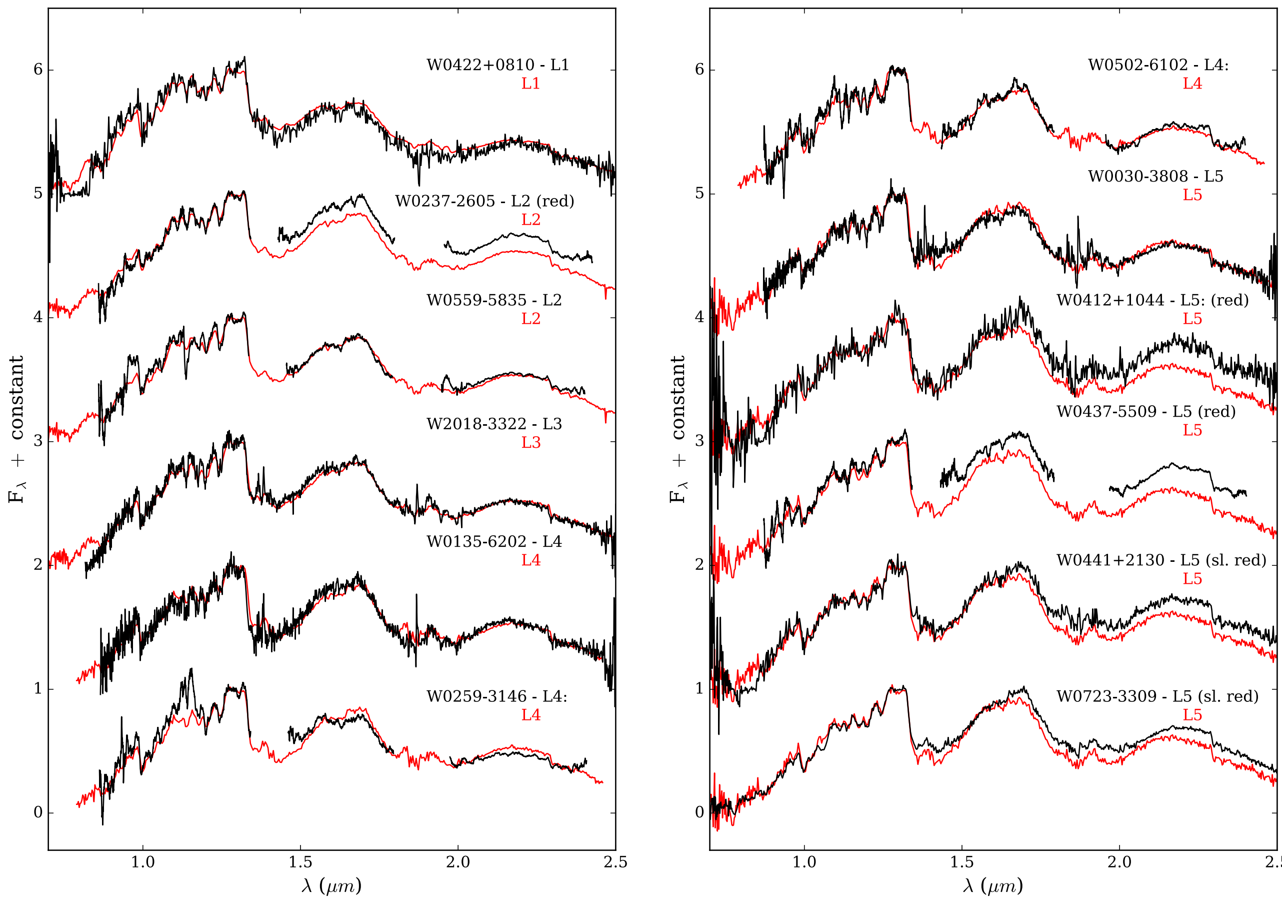

Figure 2. Near-infrared spectra of discoveries from this survey. The object spectra are plotted in black, while the closest matching near-infrared spectral standard is shown in red. All spectra are normalized between 1.27 and 1.29 μm. The standards used for comparison are as follows; L1—2MASSW J2130446−084520 (Kirkpatrick et al. 2010), L2—Kelu-1 (Burgasser et al. 2007), L3—2MASSW J1506544+132106 (Burgasser 2007), L4—2MASS J21580457−1550098 (Kirkpatrick et al. 2010), L5—SDSS J083506.16+195304.4 Chiu et al. (2006), L6—2MASSI J1010148−040649 (Reid et al. 2006b), L7—2MASSI J0103320+193536 (Cruz et al. 2004), L8—2MASSW J1632291+190441 (Burgasser 2007), L9—DENIS-P J0255−4700 (Burgasser et al. 2006).

than the calculated photometric distance. In such cases, the question of unresolved binarity would only increase photometric distance estimates, making such discrepancies worse.

The convergent point analysis tool of Rodriguez et al. (2013) uses positions and proper motions to determine motions relative to the convergent points of six different groups: AB Dor, β Pic, Carina-Near, Columba, Tuc-Hor, and TWA. We use AllWISE positions and the proper motions of each suspected young object as inputs into the convergent point tool and list the results in Table 5. We include matches with probabilities higher than 50%.

In addition to the groups listed above for BANYAN II and the convergent point tool, the LACEwING kinematic analysis tool also evaluates membership for several additional groups, including η Cha, ϵ Cha, 32 Ori, Octans, Coma Ber, Ursa Major, χ^{01} For, and the Hyades. Again, we use AllWISE positions and the proper motions listed in Table 4 to evaluate each potentially young object with LACEwING and provide the results in Table 5. All matches with probabilities >20% are provided. We note, however, that the LACEwING tool seems to be much more efficient for objects with complete kinematic information (position, proper motion, radial velocity, and parallax), while our candidates only have positions and proper motions. For example, for our newly discovered L5 (red) dwarf WISEA J235422.31−081129.7, BANYAN II finds a 94% probability of belonging to β Pic and the convergent point tool finds a probability of 100%, whereas LACEwING finds a 0% probability of belonging to β Pic. However, if we input the predicted distance and radial velocity for WISEA J235422.31 −081129.7 from BANYAN II into LACEwING, the LACEwING code finds a 60% probability of belonging to β Pic. Thus, for moving group membership evaluation, we rely primarily on results from BANYAN II and the convergent point tool and include the results from LACEwING for completeness. We list, at most, two matching associations per object per moving group evaluation tool.

5.1. Notes on Individual Objects

5.1.1. WISEA J004403.39+022810.6

This object has a high probability of belonging to β Pic according to both BANYAN II (∼78%) and the convergent point tool (∼97%). Its photometric distance (31 ± 3 pc) matches very well with the distance predicted by BANYAN II (33 ± 4 pc) and the convergent point tool (36 pc). Note that while the convergent point tool also finds a high probability of belonging to Columba (∼99%), its predicted distance if a Columba member (46 pc) is significantly different from its photometric distance.

Its spectrum shows a peaked *H*-band shape, a common feature among very young brown dwarfs, and a redder spectral

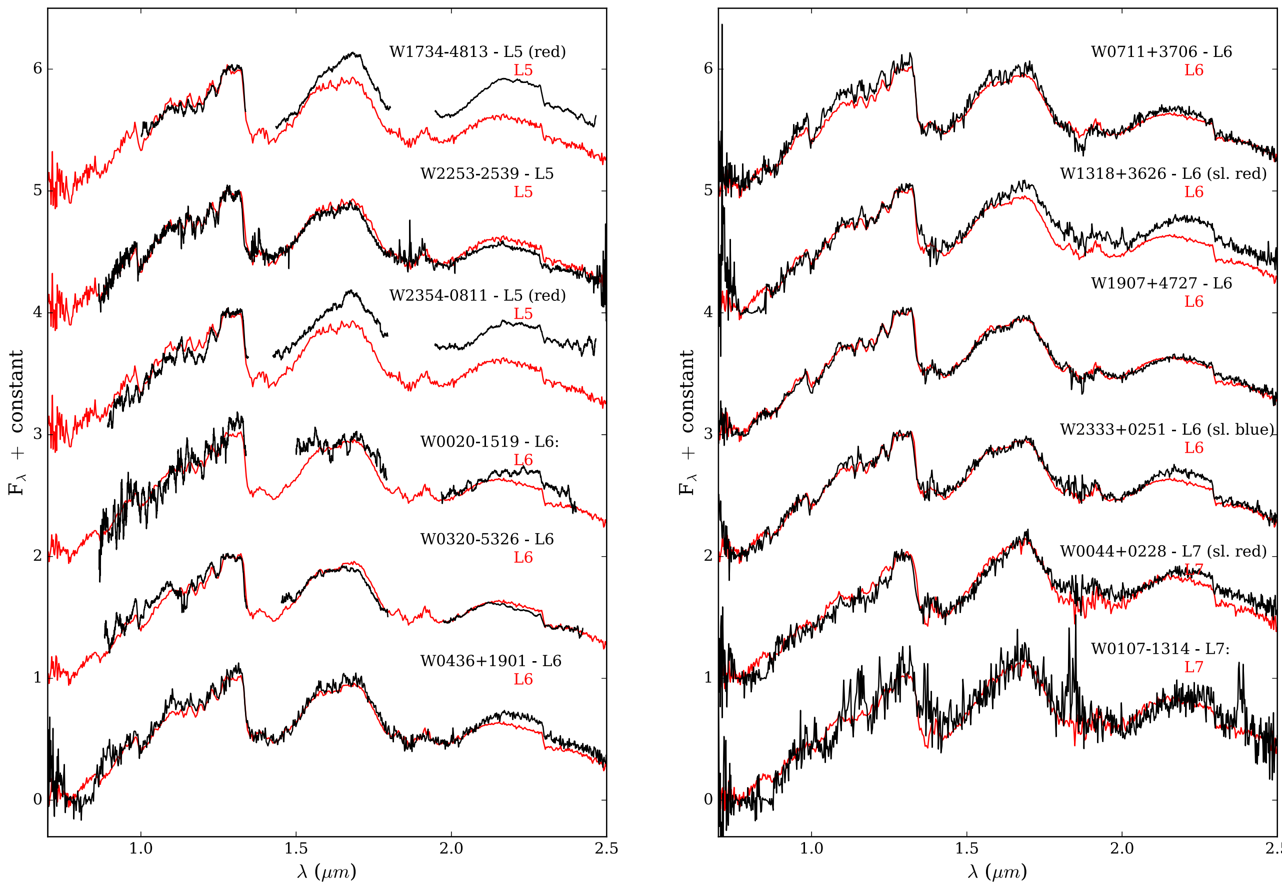

Figure 3. Same as Figure 2.

shape compared to the L7 near-infrared spectral standard. There are two spectral indices that have been shown to be effective for distinguishing young, low-gravity brown dwarfs from the field population for spectral types later than L4: the *H*-cont index (Allers & Liu 2013) and the H2(K) index (Canty et al. 2013; Schneider et al. 2014). Both indices probe areas where the effects of collisionally induced absorption of H_2 are greatly reduced in low-gravity objects, affecting their overall spectral shape. However, we note that Allers & Liu (2013) caution that the *H*-cont index is not the most reliable gravity indicator, and should be used in combination with other indices when possible. For WISEA J004403.39+022810.6, we find an *H*-cont value of 0.968 and H2(K) of 1.009, both of which align with other low-gravity objects with similar spectral types. We thus conclude that this object is a high-probability member of β Pic. Radial velocity and parallax measurements will be needed to confirm membership. If a true β Pic member, WISEA J004403.39+022810.6 would be one of the latest spectral type members known, and would hence have a very low mass. Using its photometric distance estimate, an age of 24 ± 3 Myr (Bell et al. 2015), the spectral type-K_S bolometric correction relation for young objects from Filippazzo et al. (2015), and the evolutionary models of Saumon & Marley (2008), we find a mass range of 7–11 $M_{\rm Jup}$, which would place WISEA J004403.39+022810.6 in the planetary mass regime.

While Allers & Liu (2013) provide a suggested list of low and intermediate gravity standards, they did not find suitable standards for spectral type L7. We thus compare the near-infrared spectrum of WISEA J004403.39+022810.6 to the low and intermediate surface gravity L6 standards in Figure 7.

5.1.2. WISEA J005811.69−565332.1

This object is a modest-probability member of both β Pic (∼27%) and Argus (∼31%) according to our input into BANYAN II, and has a modest probability of belonging to TucHor (∼48%) and ABDor (∼40%) according to LACEwING. Its photometric distance (22 ± 3 pc) is similar to and in between the predicted distances for both BANYAN II matched associations (19 ± 2 pc for β Pic and 25 ± 3 pc for Argus). The predicted distances for the LACEwING matches are slightly more discrepant (29 ± 3 and 29 ± 2 for TucHor and ABDor, respectively). The effects of low surface gravity on the spectral features of L9 type dwarfs has yet to be thoroughly explored, thus we cannot comment further on the youth of this object from the available spectrum. We note that a radial velocity measurement could help clear up the ambiguous moving group membership of this object, as the predicted radial velocities are 9.6, 2.5, 7.2, and 21.9 km s^{-1} for β Pic, Argus, TucHor, and ABDor, respectively.

5.1.3. WISEA J020047.29−510521.4

This object is a high-probability member of ABDor according our input into BANYAN II (∼98%), and a moderate-probability ABDor member according to the convergent point tool (∼54%) and LACEwING (∼53). Its photometric distance estimate (20 ± 2 pc) matches very well with its predicted distance if it is an ABDor member for all membership tools; 22 ± 2 pc for BANYAN II, 23 ± 2 for LACEwING, and 23 pc for the convergent point tool. Furthermore, its spectrum shows a redder than normal near-infrared shape compared to spectral standards

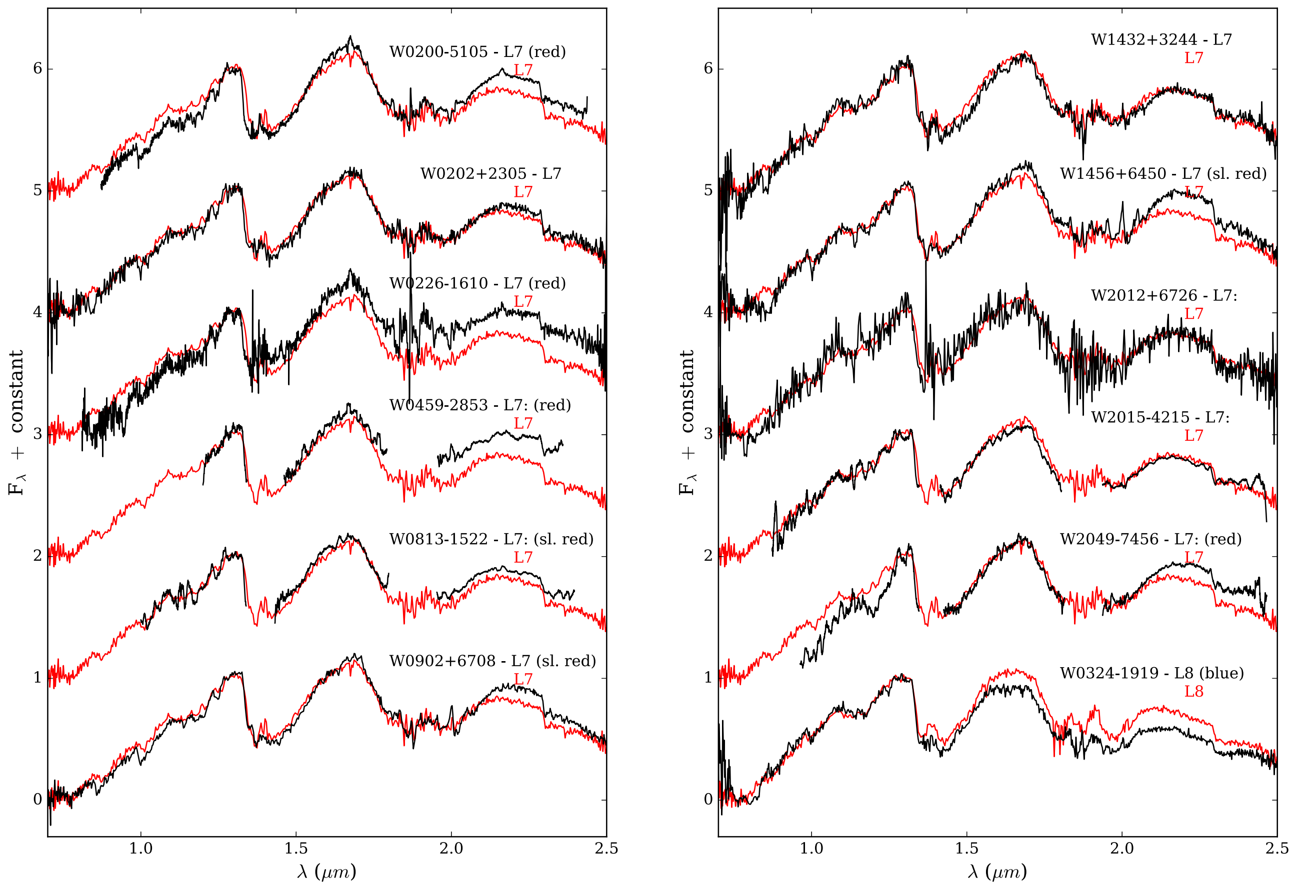

Figure 4. Same as Figure 2.

as it is one of the reddest objects in our sample ($J - K_S = 2.54$ mag). We find H-cont = 0.904 and H2(K) = 1.067, values near the boundary between field and low-gravity objects. This is consistent with the age of ABDor (∼149 Myr; Bell et al. 2015). We thus conclude that this object is a high-likelihood member of ABDor. Radial velocity and parallax measurements will be needed to confirm membership. Using the spectral type-K_S bolometric correction relation from Filippazzo et al. (2015), evolutionary models from Saumon & Marley (2008), an age of 149^{+51}_{-19} Myr (Bell et al. 2015), and WISEA J020047.29−510521.4's distance estimate, we find a mass range of 16–28 $M_{\rm Jup}$ for this object. A comparison of the near-infrared spectrum of WISEA J020047.29−510521.4 to the low and intermediate surface gravity L6 standards is shown in Figure 7.

5.1.4. WISEA J022609.16−161000.4

According to BANYAN II, this object has a high probability of belonging to ABDor (∼85%) as well as a small probability of belonging to β Pic (∼12%). The convergent point tool returns a very high probability of belonging to ABDor (∼99%), while LACEwING returns modest probabilities for both ABDor (∼36%) and TucHor (∼36%). The photometric distance estimate for this object (27 ± 3 pc) is consistent within 3σ for all three ABDor distance estimates (36 ± 3 pc, 37 ± 1 pc, and 36 pc). Its near-infrared spectrum shows a peaky H-band and a red slope compared to the L7 standard. We measure H-cont = 0.989 and H2(K) = 1.036, values consistent with other low-gravity objects. This object is also one of the reddest objects in our sample ($J - K_S = 2.74$ mag). We consider this object a high-likelihood member of ABDor. If a true member, we find a mass range of 16–28 $M_{\rm Jup}$ using the spectral type-K_S bolometric correction relation from Filippazzo et al. (2015), evolutionary models from Saumon & Marley (2008), an age of 149^{+51}_{-19} Myr (Bell et al. 2015), and WISEA J022609.16−161000.4's distance estimate. We compare the near-infrared spectrum of WISEA J022609.16−161000.4 to low and intermediate surface gravity L6 standards in Figure 7.

5.1.5. WISEA J023749.81−260543.8

This object's spectrum is significantly redder than the L2 near-infrared spectral standard. This object is not a likely member of any nearby group evaluated by BANYAN II, LACEwING, or the convergent point tool. Because it has a spectral type of ∼L2, we measure all low-gravity indices found in Allers & Liu (2013) and find values consistent with a field age population. The origin of the red near-infrared colors of this object is unknown.

5.1.6. WISEA J041232.77+104408.3

This object is red compared to the L5 near-infrared spectral standard, but does not belong to any nearby group according to BANYAN II and the convergent point tool. LACEwING, however, finds a high probability of it belonging to the Hyades cluster (∼87%). This object's photometric distance estimate (46 ± 6 pc) is fully consistent with Hyades membership, though its μ_δ value is somewhat discrepant with other Hyades members. Of the 724 Hyades members in Röser et al. (2011),

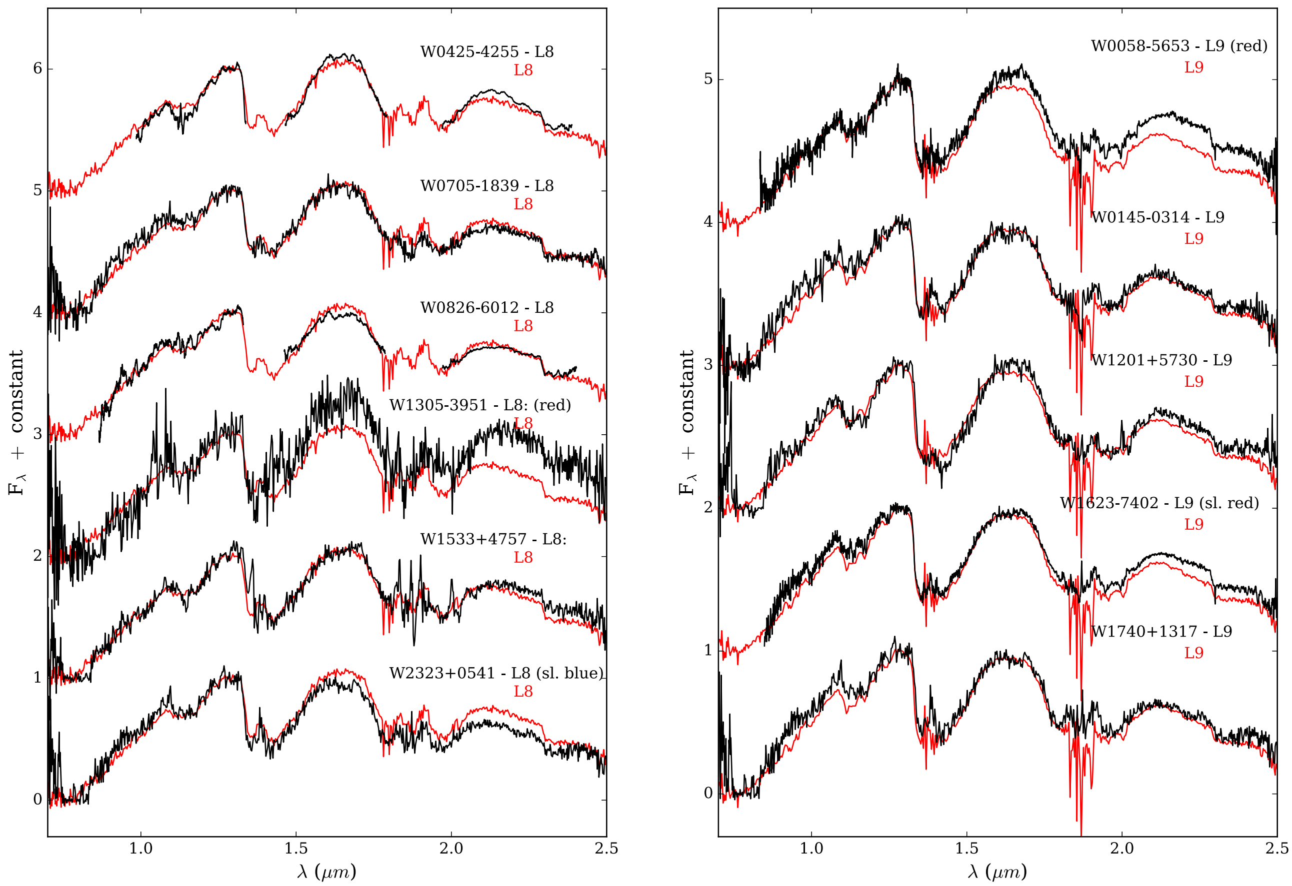

Figure 5. Same as Figure 2.

only 13 have positive μ_δ values as large as WISEA J041232.77+104408.3, all of which have negative declinations. While this does not rule out Hyades membership for this object, we consider it an unlikely member.

5.1.7. WISEA J043642.75+190134.8 and WISEA J044105.56+213001.5

These objects have sky positions coincident with the Hyades cluster. The LACEwING tool finds Hyades membership probabilities of ∼87% and 100% for WISEA J043642.75+190134.8 and WISEA J044105.56+213001.5, respectively. The photometric distance estimate of WISEA J044105.56+213001.5 (45 ± 9 pc) is well within the Hyades tidal radius of 9 pc (Röser et al. 2011) from a nominal Hyades distance of ∼47 pc (van Leeuwen 2009), and is fully consistent with the predicted LACEwING distance of 46 ± 6 pc. The photometric distance estimate of WISEA J043642.75+190134.8 (35 ± 4 pc) is 1σ from the edge of the tidal radius, and is within 2σ of the LACEwING predicted distance of 47 ± 5 pc. The average μ_α and μ_δ values for Hyades members from Röser et al. (2011) is 104.9 mas yr^{-1} and -27.3 mas yr^{-1}, respectively. We find $\mu_\alpha = 98.8 \pm 16.5$ mas yr^{-1} and $\mu_\delta = -29.0 \pm 12.5$ mas yr^{-1} for WISEA J043642.75+190134.8 and $\mu_\alpha = 98.1 \pm 27.3$ mas yr^{-1} and $\mu_\delta = -39.0 \pm 23.2$ mas yr^{-1} for WISEA J044105.56+213001.5, both consistent with other Hyades members. At L5 and L6, these would be the latest spectral type members of the Hyades with the exceptions of CFHT-Hy-20 (Bouvier et al. 2008), recently confirmed as a T2 spectral type member in Liu et al. (2016) and 2MASS J04183483+2131275, a recently confirmed L5 Hyades member (Pérez-Garrido et al. 2017).

5.1.8. WISEA J043718.77−550944.0

This object's spectrum is very red compared to the L5 spectral standard, and according to BANYAN II and the convergent point tool, is a high probability member of β Pic (∼94% and ∼93%, respectively). However, the predicted distances (17 ± 3 pc and 19 pc) do not agree with the estimated photometric distance (35 ± 7 pc). We measure an H-cont value of 0.975, consistent with having a low gravity, but measure $H2(K) = 1.064$, which is indicative of a field age gravity. This object is worthy of additional observations to untangle its potential youth and moving group membership.

5.1.9. WISEA J045900.42−285338.3

According to BANYAN II, this object has a modest probability of belonging to both β Pic (∼29%) and Argus (∼55%). However, the predicted distances in both cases do not agree with the estimated photometric distance. The convergent point tool finds a large probability of belonging to Carina-Near (∼97%) and a distance within 2σ of its photometric distance estimate. However, we note that the sky position of WISEA J045900.42−285338.3 is not near to any of the proposed Carina-Near members in Zuckerman et al. (2006). We measure H-cont $= 0.943$ and $H2(K) = 1.012$, values consistent with having a low surface gravity. This object may belong to an as yet unknown group.

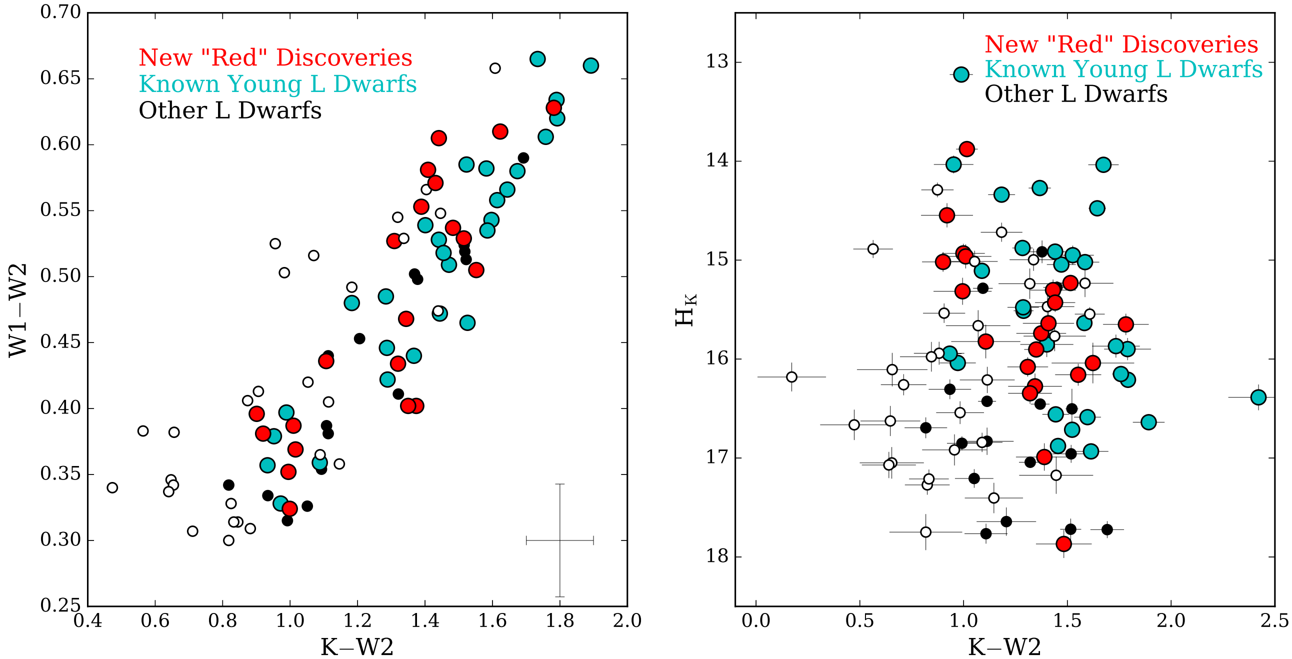

Figure 6. Left: color–color diagram comparing the discoveries from this survey to previously known young brown dwarfs. The typical uncertainty for each plotted symbol is shown in the bottom right corner. Right: reduced proper motion diagram comparing the discoveries from this survey to previously known young brown dwarfs. The discoveries with "red" or "sl. red" spectral types are shown at red symbols, while known young L dwarfs are shown in cyan. All other plotted objects have no signs of youth in their spectra; both new discoveries (open symbols) and previously known brown dwarfs (filled black symbols). WISEA J114724.10−204021.3, which was discovered as part of this survey but published separately (Schneider et al. 2016b) is plotted as a red symbol.

5.1.10. WISEA J072352.62−330943.5

This object has a reasonable probability of belonging to Argus according to BANYAN II (∼53%) and LACEwING (∼25%) and its spectrum is redder than the near-infrared L5 standard. Note that the convergent point tool does not consider the Argus moving group. Its distance estimate from photometry (23 ± 2 pc) is in good agreement with the BANYAN predicted distance if an Argus member (26 ± 4 pc). We find H-cont = 0.923 and H2(K) = 1.031, values consistent with an intermediate to low surface gravity. We suggest this object is a medium-to-high probability member of Argus. If an Argus member, with an age of ∼40 Myr (Torres et al. 2008), then it would have a mass of 11–12 $M_{\rm Jup}$, using its distance estimate, the spectral type-K_S bolometric correction relation from Filippazzo et al. (2015), and evolutionary models from Saumon & Marley (2008).

5.1.11. WISEA J081322.19−152203.2

This object's spectrum is slightly red compared to the L7 near-infrared standard. It is a high-probability member of Argus (∼87%), according to BANYAN II, and Carina-Near (∼97%), according to the convergent point tool, but its photometric distance estimate (31 ± 6 pc) is significantly different than the BANYAN II predicted distance (15 ± 2 pc) and the convergent point tool distance (17 pc). We find H-cont = 0.941, consistent with a low surface gravity, but find H2(K) = 1.054, which coincides with field age objects. The age of this object remains ambiguous.

5.1.12. WISEA J090258.99+670833.1

This object's spectrum is slightly red compared to the L7 near-infrared standard. It is a fairly high probability member of ABDor (∼56%) according to BANYAN II and its predicted distance (23 ± 2 pc) is a perfect match to its photometric distance (23 ± 2 pc). However, the convergent point tool find a high probability of belonging to Columba (∼83%) with a similar distance. Note that both LACEwING and the convergent point tool find probabilities of belonging to ABDor just below our threshold (∼14% and ∼46%, respectively) and predict a distance of ∼24 pc. This object is one of the reddest objects in our sample ($J - K_S = 2.73$ mag). We measure H-cont = 0.918 and H2(K) = 1.014, values completely consistent with having a low surface gravity. We conclude this object is a medium-to-high probability ABDor member. Using the spectral type-K_S bolometric correction relation from Filippazzo et al. (2015), evolutionary models from Saumon & Marley (2008), an age of 149^{+51}_{-19} Myr (Bell et al. 2015), and a distance estimate of 23.4 pc, we find a mass range of 16–28 $M_{\rm Jup}$ if a true ABDor member. A comparison of the near-infrared spectrum of WISEA J090258.99+670833.1 to the low and intermediate surface gravity L6 standards in shown in Figure 7.

5.1.13. WISEA J130523.06−395104.9

This object's spectrum is red compared to the near-infrared L8 standard, but is rather noisy, so the spectral type is uncertain. It has a large probability of belonging to Argus (∼95%) according to BANYAN II, but its predicted distance (21 ± 2 pc) differs from its photometric distance estimate (30 ± 5 pc). The convergent point tool returns possible membership in TucHor (∼80%) and Carina-Near (∼59%), though the distance estimate if a TucHor member (18 pc) and the sky position compared to Carina-Near members from Zuckerman et al. (2006) makes membership in either unlikely. We retain this object as a possible Argus member. A higher S/N spectrum would help to confirm this object's youth.

Table 5
Moving Group Membership Summary

AllWISE Designation	BANYAN II (%)	d_{pred} [a] (pc)	LACEwING (%)	d_{pred} [a] (pc)	CP (%)	d_{pred} [a] (pc)
J004403.39+022810.6	β Pic (78)	33 ± 4	...	...	Columba (99), β Pic (97)	46, 36
J005811.69−565332.1	β Pic (27), Argus (31)	19 ± 2, 25 ± 3	TucHor (48), ABDor (40)	29 ± 3, 29 ± 2	Car-Near (50)	33
J020047.29−510521.4	ABDor (98)	22 ± 2	TucHor (28), ABDor (53)	24 ± 3, 23 ± 2	ABDor (54)	23
J022609.16−161000.4	β Pic (12), ABDor (85)	23 ± 3, 36 ± 3	TucHor (36), ABDor (36)	34 ± 3, 37 ± 1	ABDor (99)	36
J023749.81−260543.8	...	...	...	...	...	...
J041232.77+104408.3	...	...	Hyades (87)	49 ± 13	...	...
J043642.75+190134.8	...	...	Hyades (87)	47 ± 5	Car-Near (55)	37
J043718.77−550944.0	β Pic (94)	17 ± 3	TucHor (20), ABDor (20)	32 ± 9, 18 ± 6	β Pic (93), TWA (88)	19, 22
J044105.56+213001.5	Argus (14)	22 ± 5	Hyades (100)	46 ± 6	Car-Near (74)	36
J045900.42−285338.3	β Pic (29), Argus (55)	9 ± 3, 19 ± 4	...	...	Car-Near (97)	28
J072352.62−330943.5	Argus (53)	26 ± 4	Argus (25)	31 ± 2	Car-Near (97)	36
J081322.19−152203.2	Argus (87)	15 ± 2	...	...	Car-Near (97)	17
J090258.99+670833.1	ABDor (56)	23 ± 2	...	...	Columba (83)	23
J130523.06−395104.9	Argus (95)	21 ± 2	...	...	TucHor (80), Car-Near (59)	18, 27
J131845.58+362614.0	...	...	...	...	Car-Near (90)	72
J145642.68+645009.7	ABDor (52)	16 ± 2	...	...	ABDor (71), Columba (65)	17, 21
J162341.27−740230.4	β Pic (58), ABDor (36)	11 ± 1, 14 ± 1	Argus (32), ABDor (38)	13 ± 1, 14 ± 2	ABDor (70)	14
J173453.90−481357.9	Argus (45)	13 ± 2	Argus (36), ABDor (24)	17 ± 2, 28 ± 2	Car-Near (63)	20
J204902.80−745613.5	β Pic (29), TucHor (42)	29 ± 4, 49 ± 5	TucHor (31), ABDor (22)	37 ± 7, 42 ± 3	Columba (98), TucHor (81)	42, 37
J235422.31−081129.7	β Pic (94)	29 ± 3	ABDor (23)	47.5 ± 1	β Pic (100), TWA (96)	30, 31

Note.
[a] Predicted distance if indeed a member of the moving group (or groups) listed in the "BANYAN II," "LACEwING," or "CP" columns. If more than one value is listed, their order corresponds to the order of groups listed in the previous column.

5.1.14. WISEA J131845.58+362614.0

This object's spectrum is red compared to the L6 spectral standard, but does not seem to belong to any nearby group according to BANYAN II. The convergent point tool finds a high probability of belonging to Carina-Near (∼90%), though its distance estimate (72 pc) compared to its photometric distance (40 ± 5 pc) makes membership unlikely. We find H-cont = 0.930 and H2(K) = 1.006, values consistent with young, low-gravity objects. This object may belong to an as yet unknown, young, nearby group.

5.1.15. WISEA J145642.68+645009.7

This object's spectrum is slightly red compared to the L7 near-infrared spectral standard. It has a good probability of belonging to ABDor according to BANYAN II (∼52%) and the convergent point tool (∼71%). This object is also one of the reddest objects in our sample ($J - K_S = 2.79$ mag). The photometric distance of this object (30 ± 3 pc) and predicted distances (16 ± 2 pc and 17 pc) do not agree, however. We measure H-cont = 0.910 and H2(K) = 1.044, consistent with an intermediate surface gravity. The youth of this object remains ambiguous.

5.1.16. WISEA J162341.27−740230.4

This object has a moderate probability of belong to either β Pic or ABDor according to BANYAN II (58% and 36%, respectively), Argus and ABDor according to LACEwING (∼32% and ∼38%, respectively), and ABDor (∼70%) according to the convergent point tool. However, its photometric distance estimate (26 ± 3 pc) is much further than the predicted distances for all of these groups, and thus unlikely to be a member of any of them.

5.1.17. WISEA J173453.90−481357.9

This object's spectrum is very red compared to the L5 spectral standard. BANYAN II suggests that this object may belong to Argus (∼45%), but its photometric distance (25 ± 2 pc) does not match well with its predicted distance (13 ± 2 pc). LACEwING also suggests possible Argus membership (∼36%) as well as ABDor (∼24%), while the convergent point tool suggests membership in Carina-Near (∼63%). The predicted ABDor distance from LACEwING (28 ± 2 pc) is consistent with this object's photometric distance. However, because both BANYAN II and the convergent point tool give ABDor probabilities of 0%, we consider this object a low-probability ABDor member. Its measured values of H-cont = 0.939 and H2(K) = 1.032 suggest an intermediate surface gravity.

5.1.18. WISEA J204902.80−745613.5

This object is redder than the L7 spectral standard and has a moderate probability of belonging to TucHor according to BANYAN II (∼42%), LACEwING (∼31%), and the convergent point tool (∼81%). While its photometric distance estimate of 37 ± 5 pc disagrees with the predicted distance from BANYAN II for TucHor (49 ± 5 pc), it agrees almost perfectly with the predicted distances from LACEwING (37 ± 7 pc) and the convergent point tool (37 pc). We thus conclude that this is a moderate-probability TucHor member worthy of additional follow up observations. If confirmed as at TucHor member, this would be the latest spectral type member known. We measure H-cont = 0.938 and H2(K) = 1.010, consistent with a low surface gravity. We compare the near-infrared spectrum of WISEA J204902.80−745613.5 to low and intermediate surface gravity L6 standards in Figure 7.

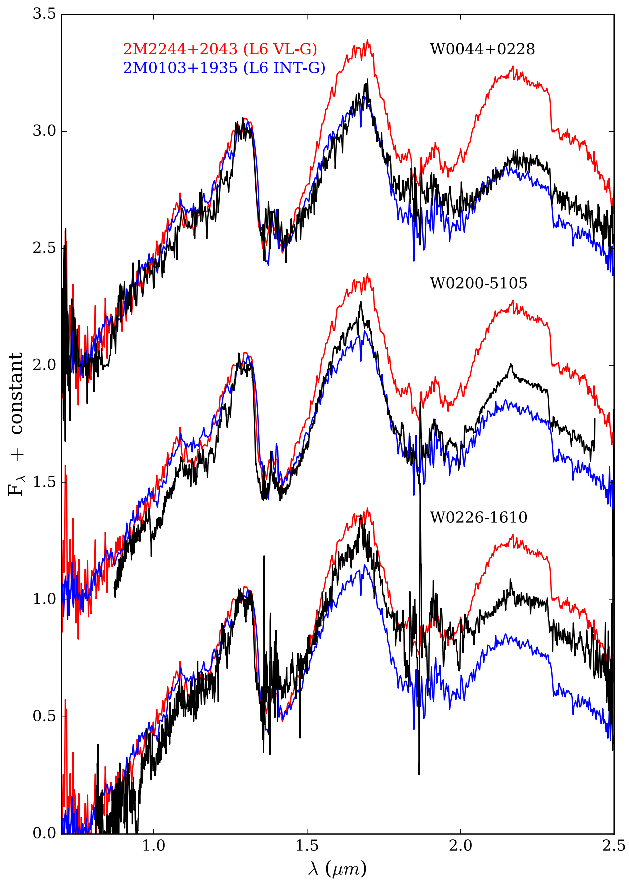

Figure 7. Near-infrared spectra of several newly proposed moving group members discovered with this survey compared to the low gravity standards suggested in Allers & Liu (2013). All spectra are normalized between 1.27 and 1.29 μm. The standards used for comparison are 2MASSI J0103320+193536 (L6 INT-G; Cruz et al. 2004) and 2MASSW J2244316+204343 (L6 VL-G; Looper et al. 2008).

5.1.19. WISEA J235422.31−081129.7

This object is very red compared to the L5 spectral standard. It is a high-probability member of β Pic according to both BANYAN II (∼94%) and the convergent point (100%). Its photometric distance (38 ± 5) is within 2σ of its predicted distance in both instances (29 ± 3 pc and 30 pc). We measure H-cont = 0.991 and H2(K) = 1.034, values consistent with a low gravity. We consider this object a high-probability member of β Pic. We use its photometric distance estimate, an age of 24 ± 3 Myr (Bell et al. 2015), the spectral type-K_S bolometric correction relation for young objects from Filippazzo et al. (2015), and the evolutionary models of Saumon & Marley (2008) to find a mass range of 9−12 M_{Jup}, placing WISEA J235422.31−081129.7 in the planetary mass regime if a true β Pic member. Allers & Liu (2013) did not find suitable low and intermediate gravity standards for spectral type L5. We thus compare the near-infrared spectrum of WISEA J235422.31 −081129.7 to the low and intermediate surface gravity L6 standards in Figure 7.

6. Conclusions

We have used the unique near- and mid-infrared colors of young, late-type L dwarfs to identify 50 new late-type L dwarf candidates, 47 of which we have confirmed spectroscopically as L dwarfs. We assert that two objects (WISEA J004403.39 +022810.6 and WISEA J235422.31−081129.7) are likely β Pic members based on their membership probabilities from BANYAN II and the convergent point tool of Rodriguez et al. (2013), youthful spectroscopic characteristics, and distance estimates. If true β Pic members, we estimate that both of these objects have masses in the planetary mass regime. We also find three highly likely members of ABDor (WISEA J020047.29−510521.4, WISEA J022609.16−161000.4, and WISEA J090258.99+670833.1), one medium-to-high probability member of Argus (WISEA J072352.62−330943.5), and one moderate-probability member of TucHor (WISEA J204902.80−745613.5). We have also identified two potential late-L type Hyades members (WISEA J043642.75+190134.8 and WISEA J044105.56+213001.5). These objects, if confirmed, would be some of the lowest mass members of these groups. Because brown dwarfs cool as they age, they do not obey a simple mass–luminosity relationship like stars. Instead, brown dwarfs follow a mass–luminosity–age relation, making age a vital parameter for the determination of brown dwarf physical properties. This sample of newly discovered potential moving group and cluster members thus provides indispensable benchmarks for investigating the evolution of low-mass objects and constraining low-mass evolutionary models.

The limiting factor in this search was the depth of the 2MASS catalog. Expanding this search to include deeper near-infrared catalogs, such as UKIDSS (Lawrence et al. 2007) or the VISTA Hemisphere Survey (VHS; PI: McMahon, Cambridge, UK) would undoubtedly reveal more late-L type members of the Solar neighborhood.

A.S. and E.S. appreciate support from NASA grant NNX16AB62G. The authors would like to thank Katelyn Allers for help with the ARCoIRIS observations and the reduction of ARCoIRIS and FIRE data, and Scott Sheppard for useful discussions regarding FIRE observations. This paper includes data gathered with the 6.5 meter *Magellan* Telescopes located at Las Campanas Observatory, Chile and is based in part on observations at Cerro Tololo Inter-American Observatory, National Optical Astronomy Observatory (NOAO Prop. ID: 2016B-0003; PI: A. Schneider), which is operated by the Association of Universities for Research in Astronomy (AURA) under a cooperative agreement with the National Science Foundation. This publication makes use of data products from the *Wide-field Infrared Survey Explorer*, which is a joint project of the University of California, Los Angeles, and the Jet Propulsion Laboratory/California Institute of Technology. *WISE* is funded by the National Aeronautics and Space Administration. This publication makes use of data products from the Two Micron All Sky Survey, which is a joint project of the University of Massachusetts and the Infrared Processing and Analysis Center/California Institute of Technology, funded by the National Aeronautics and Space Administration and the National Science Foundation. This research has made use of the SIMBAD database, operated at CDS, Strasbourg, France. This research has benefitted from the M, L, T, and Y dwarf compendium housed at dwarfarchives.org. The authors wish to recognize and acknowledge the very significant cultural role and reverence that the summit of Mauna Kea has always had within the indigenous Hawaiian community. We are most fortunate to have the opportunity to conduct observations from this mountain.

References

Aller, K. M., Liu, M. C., Magnier, E. A., et al. 2016, ApJ, 821, 120
Allers, K. N., & Liu, M. C. 2013, ApJ, 772, 79
Bell, C. P. M., Mamajek, E. E., & Naylor, T. 2015, MNRAS, 454, 593
Best, W. M. J., Liu, M. C., Magnier, E. A., et al. 2015, ApJ, 814, 118
Bouvier, J., Kendall, T., Meeus, G., et al. 2008, A&A, 481, 661
Burgasser, A. J. 2007, ApJ, 659, 655
Burgasser, A. J., Geballe, T. R., Leggett, S. K., Kirkpatrick, J. D., & Golimowski, D. A. 2006, ApJ, 637, 1067
Burgasser, A. J., Looper, D. L., Kirkpatrick, J. D., & Liu, M. C. 2007, ApJ, 658, 557
Canty, J. I., Lucas, P. W., Roche, P. F., & Pinfield, D. J. 2013, MNRAS, 435, 2650
Chiu, K., Fan, X., Leggett, S. K., et al. 2006, AJ, 131, 2722
Cruz, K. L., Burgasser, A. J., Reid, I. N., & Liebert, J. 2004, ApJL, 604, L61
Cruz, K. L., Kirkpatrick, J. D., & Burgasser, A. J. 2009, AJ, 137, 3345
Cruz, K. L., Reid, I. N., Kirkpatrick, J. D., et al. 2007, AJ, 133, 439
Cruz, K. L., Reid, I. N., Liebert, J., Kirkpatrick, J. D., & Lowrance, P. J. 2003, AJ, 126, 2421
Cushing, M. C., Vacca, W. D., & Rayner, J. T. 2004, PASP, 116, 362
Dahn, C. C., Harris, H. C., Vrba, F. J., et al. 2002, AJ, 124, 1170
Dupuy, T. J., & Liu, M. C. 2012, ApJS, 201, 19
Faherty, J. K., Burgasser, A. J., Walter, F. M., et al. 2012, ApJ, 752, 56
Faherty, J. K., Rice, E. L., Cruz, K. L., Mamajek, E. E., & Núñez, A. 2013, AJ, 145, 2
Faherty, J. K., Riedel, A. R., Cruz, K. L., et al. 2016, ApJS, 225, 10
Filippazzo, J. C., Rice, E. L., Faherty, J., et al. 2015, ApJ, 810, 158
Gagné, J., Faherty, J. K., Cruz, K. L., et al. 2015, ApJS, 219, 33
Gagné, J., Faherty, J. K., Mamajek, E. E., et al. 2017, ApJS, 228, 18
Gagné, J., Lafrenière, D., Doyon, R., et al. 2014a, ApJL, 792, L17
Gagné, J., Lafrenière, D., Doyon, R., Malo, L., & Artigau, É. 2014b, ApJ, 783, 121
Gagné, J., Lafrenière, D., Doyon, R., Malo, L., & Artigau, É. 2015, ApJ, 798, 73
Gauza, B., Béjar, V. J. S., Pérez-Garrido, A., et al. 2015, ApJ, 804, 96
Geballe, T. R., Knapp, G. R., Leggett, S. K., et al. 2002, ApJ, 564, 466
Gizis, J. E., Allers, K. N., Liu, M. C., et al. 2015, ApJ, 799, 203
Gizis, J. E., Faherty, J. K., Liu, M. C., et al. 2012, AJ, 144, 94
Gizis, J. E., Reid, I. N., Knapp, G. R., et al. 2003, AJ, 125, 3302
Hogan, E., Jameson, R. F., Casewell, S. L., Osbourne, S. L., & Hambly, N. C. 2008, MNRAS, 388, 495
Kellogg, K., Metchev, S., Gagné, J., & Faherty, J. 2016, ApJL, 821, L15
Kellogg, K., Metchev, S., Geissler, K., et al. 2015, AJ, 150, 182
Kirkpatrick, J. D., Barman, T. S., Burgasser, A. J., et al. 2006, ApJ, 639, 1120
Kirkpatrick, J. D., Cruz, K. L., Barman, T. S., et al. 2008, ApJ, 689, 1295
Kirkpatrick, J. D., Cushing, M. C., Gelino, C. R., et al. 2011, ApJS, 197, 19
Kirkpatrick, J. D., Kellogg, K., Schneider, A. C., et al. 2016, ApJS, 224, 36
Kirkpatrick, J. D., Looper, D. L., Burgasser, A. J., et al. 2010, ApJS, 190, 100
Kirkpatrick, J. D., Reid, I. N., Liebert, J., et al. 1999, ApJ, 519, 802
Kirkpatrick, J. D., Reid, I. N., Liebert, J., et al. 2000, AJ, 120, 447
Knapp, G. R., Leggett, S. K., Fan, X., et al. 2004, AJ, 127, 3553
Lawrence, A., Warren, S. J., Almaini, O., et al. 2007, MNRAS, 379, 1599
Liebert, J., & Gizis, J. E. 2006, PASP, 118, 659
Liu, M. C., Dupuy, T. J., & Allers, K. N. 2016, ApJ, 833, 96
Liu, M. C., Magnier, E. A., Deacon, N. R., et al. 2013, ApJL, 777, L20
Lodieu, N., Boudreault, S., & Béjar, V. J. S. 2014, MNRAS, 445, 3908
Looper, D. L., Kirkpatrick, J. D., Cutri, R. M., et al. 2008, ApJ, 686, 528
Luhman, K. L. 2014, ApJ, 781, 4
Mace, G. N., Kirkpatrick, J. D., Cushing, M. C., et al. 2013, ApJS, 205, 6
Malo, L., Doyon, R., Lafrenière, D., et al. 2013, ApJ, 762, 88
Marocco, F., Day-Jones, A. C., Lucas, P. W., et al. 2014, MNRAS, 439, 372
Metchev, S. A., Kirkpatrick, J. D., Berriman, G. B., & Looper, D. 2008, ApJ, 676, 1281
Pérez-Garrido, A., Lodieu, N., & Rebolo, R. 2017, A&A, 599, A78
Rayner, J. T., Toomey, D. W., Onaka, P. M., et al. 2003, PASP, 115, 362
Rebolo, R., Zapatero Osorio, M. R., Madruga, S., et al. 1998, Sci, 282, 1309
Reid, I. N., Cruz, K. L., Kirkpatrick, J. D., et al. 2008, AJ, 136, 1290
Reid, I. N., Lewitus, E., Allen, P. R., Cruz, K. L., & Burgasser, A. J. 2006a, AJ, 132, 891
Reid, I. N., Lewitus, E., Burgasser, A. J., & Cruz, K. L. 2006b, ApJ, 639, 1114
Riedel, A. R., Blunt, S. C., Lambrides, E. L., et al. 2017, AJ, 153, 95
Robert, J., Gagné, J., Artigau, É, et al. 2016, ApJ, 830, 144
Rodriguez, D. R., Zuckerman, B., Kastner, J. H., et al. 2013, ApJ, 774, 101
Röser, S., Schilbach, E., Piskunov, A. E., Kharchenko, N. V., & Scholz, R.-D. 2011, A&A, 531, A92
Saumon, D., & Marley, M. S. 2008, ApJ, 689, 1327
Schneider, A. C., Cushing, M. C., Kirkpatrick, J. D., et al. 2014, AJ, 147, 34
Schneider, A. C., Greco, J., Cushing, M. C., et al. 2016a, ApJ, 817, 112
Schneider, A. C., Windsor, J., Cushing, M. C., Kirkpatrick, J. D., & Wright, E. L. 2016b, ApJL, 822, L1
Simcoe, R. A., Burgasser, A. J., Schechter, P. L., et al. 2013, PASP, 125, 270
Skrutskie, M. F., Cutri, R. M., Stiening, R., et al. 2006, AJ, 131, 1163
Skrzypek, N., Warren, S. J., & Faherty, J. K. 2016, A&A, 589, A49
Thompson, M. A., Kirkpatrick, J. D., Mace, G. N., et al. 2013, PASP, 125, 809
Torres, C. A. O., Quast, G. R., Melo, C. H. F., & Sterzik, M. F. 2008, in Handbook of Star Forming Regions, Volume II: The Southern Sky, Vol. 5, ed. B. Reipurth (San Francisco, CA: ASP), 757
Vacca, W. D., Cushing, M. C., & Rayner, J. T. 2003, PASP, 115, 389
van Leeuwen, F. 2009, A&A, 497, 209
Wright, E. L., Eisenhardt, P. R. M., Mainzer, A. K., et al. 2010, AJ, 140, 1868
Zakhozhay, O. V., Zapatero Osorio, M. R., Béjar, V. J. S., & Boehler, Y. 2017, MNRAS, 464, 1108
Zhang, Z. H., Pokorny, R. S., Jones, H. R. A., et al. 2009, A&A, 497, 619
Zuckerman, B., Bessell, M. S., Song, I., & Kim, S. 2006, ApJL, 649, L115